



Full length article

The mixed marriage of copper and carbon ring- $g\text{-C}_3\text{N}_4$ nanosheet: A visible-light-driven heterogeneous Fenton-like catalystLingli Wang^a, Yu Zhu^a, Dan Yang^a, Lei Zhao^a, Hanming Ding^{a,*}, Zhaohui Wang^{b,c,**}^a School of Chemistry and Molecular Engineering, East China Normal University, Shanghai 200241, China^b School of Ecological and Environmental Sciences, Shanghai Key Laboratory for Urban Ecological Process and Eco-Restoration, East China Normal University, Shanghai 200241, China^c Institute of Eco-Chongming (IEC), Shanghai 200062, China

ARTICLE INFO

Keywords:

Carbon ring
Copper
Fenton-like
Synergy
Photodegradation

ABSTRACT

Effective photogenerated charge separation and rapid Cu(II)/Cu(I) redox cycling is still challenging for photocatalytic reactions and copper-based Fenton-like process, respectively. Herein, a novel heterogeneous Fenton-like catalyst of copper incorporated carbon ring- $g\text{-C}_3\text{N}_4$ (Cu-C-CN) was prepared through a facile calcination method. The carbon ring could be intimately connected with $g\text{-C}_3\text{N}_4$ via sp^2 -hybridized C–N bonds to form an in-plane π -conjugated structure. The carbon ring spliced $g\text{-C}_3\text{N}_4$ (C-CN) can serve as an effective electron-hole separator owing to the varied electron affinity of two domains (e.g. carbon-ring and $g\text{-C}_3\text{N}_4$). The copper species were further introduced to the framework of $g\text{-C}_3\text{N}_4$ via the Cu–N bonds to act as acceptors of conduction-electrons from $g\text{-C}_3\text{N}_4$ and H_2O_2 activators. Taking the photodegradation of methylene blue (MB) as a model reaction, the decomposition efficiency over Cu-C-CN is 5.5 times higher than that of pristine $g\text{-C}_3\text{N}_4$, and would nearly linearly increase with pH. The notable enhancement in photodegradation efficiency could be ascribed to the synergetic collaboration between photocatalysis process and Fenton-like process to generate abundant $\cdot\text{OH}$ and e^- . The Cu-C-CN catalyst shows high recycling stability with negligible Cu leaching due to the strong affinity of Cu^{2+} to $g\text{-C}_3\text{N}_4$ framework. The strategy of coupling Fenton-like catalysts, electron-deficient domains (e.g. carbon-ring) into semiconductor-based photocatalysis provides a facile and promising solution to the remediation of water pollution with solar energy.

1. Introduction

Recently, graphitic carbon nitride ($g\text{-C}_3\text{N}_4$) based photocatalysts have attracted increasing interest since Wang and his coworkers first discovered the photocatalytic water splitting over $g\text{-C}_3\text{N}_4$ in 2009 [1]. To date, significant progress has been achieved on the photocatalytic applications in direct solar water splitting, degradation of pollutants and CO_2 reduction due to its appealing features, such as low cost, favorable band gap and good stability [2–4]. Importantly, as a metal-free polymeric semiconductor, $g\text{-C}_3\text{N}_4$ can be readily tailored to develop hybrid photocatalysts with controllable sizes, thickness, morphologies and compositions [5]. However, the short lifetime of photo-generated electrons and marginal visible light absorption substantially constrains the photocatalytic activity of pristine $g\text{-C}_3\text{N}_4$ [6,7]. To overcome these issues, various approaches have been devoted to modifying the atomic and electronic structures of $g\text{-C}_3\text{N}_4$ via element doping or heterostructure

fabrication [8–10]. Zhu et al. has synthesized P-doped $g\text{-C}_3\text{N}_4$ through a co-condensation route to modify its electronic structure for photocatalytic hydrogen evolution [11]. Li et al. also found a novel O-doped $g\text{-C}_3\text{N}_4$ with good visible-light reactivity because of the modulated band structure [12].

Recently Che et al. designed an in-plane graphitic carbon ring (C_{ring})- $g\text{-C}_3\text{N}_4$ π -conjugated heterostructure via seamlessly stitching two-dimensional domains to synergistically broaden the light responsive range of $g\text{-C}_3\text{N}_4$ and expedite the electron-hole pair separation and transportation [13]. This novel heterostructural nanosheet displayed significantly higher photocatalytic water splitting activity under full solar spectrum than most of other photocatalysts, because: 1) a new intermediate energy level above the valence band is created owing to the interaction coupling of triazine and in-plane carbon ring, which allows for utilization of visible light with lower energy; 2) the local in-plane π -conjugated electric field enables a dramatic increase in the

* Corresponding author.

** Correspondence to: Z. Wang, School of Ecological and Environmental Sciences, Shanghai Key Laboratory for Urban Ecological Process and Eco-Restoration, East China Normal University, Shanghai 200241, China.

E-mail addresses: hmding@chem.ecnu.edu.cn (H. Ding), zhwang@des.ecnu.edu.cn (Z. Wang).<https://doi.org/10.1016/j.apsusc.2019.05.288>

Received 8 January 2019; Received in revised form 1 May 2019; Accepted 24 May 2019

Available online 25 May 2019

0169-4332/ © 2019 Elsevier B.V. All rights reserved.

spatial charge separation efficiency; 3) surface adsorption and reduction of H^+ are enhanced, thereby effectively avoiding surface charge recombination. Despite the success of $(C_{ring})-C_3N_4$ in photocatalytic water splitting, our preliminary data indicate the degradation efficiency of methylene blue (MB) using this material was not satisfactory. Therefore, $(C_{ring})-C_3N_4$ heterostructure still needs further modification if its environmental application is considered.

In addition to photocatalytic oxidation, other advanced oxidation processes (AOPs) have been well demonstrated to be effective treatments for a wide range of recalcitrant organic pollutants [14,15]. For example, heterogeneous Fenton-like process is regarded as an effective way for the generation of highly reactive and non-selective $\cdot OH$ [16–19]. Various multivalent metal species, such as cobalt, iron, copper and manganese [20–22], have been considered to be efficient catalysts to activate H_2O_2 via Fenton-like process. In addition to the widely used Fe-based catalysts, Cu-containing material has attracted increasing attention because redox properties of copper (Cu(I)/Cu(II)) are similar to iron (Fe(II)/Fe(III)) and Cu-based catalysts are able to work over a broader pH range than Fe-based materials. More importantly, the reaction of Cu(I) with H_2O_2 ($k = 1 \times 10^4 M^{-1} s^{-1}$) to produce $\cdot OH$ occurs more rapidly than that of Fe(II)- H_2O_2 system ($k = 76 M^{-1} s^{-1}$) [18], while reduction of Cu(II) to Cu(I) by H_2O_2 ($k = 4.6 \times 10^2 M^{-1} s^{-1}$) becomes more easily than that of Fe(III) back to Fe(II) ($k = 0.001-0.01 M^{-1} s^{-1}$) [23,24]. To date, lots of Cu-based catalysts, such as Cu_2O-Cu/C [25], $CuCr_2O_4/g-C_3N_4-NS$ [26] and Cu-doped $LaFeO_3$ [27], have been developed. In this context, copper-based Fenton-like system is hypothesized to enhance the catalytic performance of $(C_{ring})-C_3N_4$ owing to the combination of photocatalysis and Fenton-like process [28,29]. $g-C_3N_4$ possesses tunable electronic properties and ideal nitrogen-sites, which can effectively trap metal atoms to serve as reactive sites, and chemically stable due to the ligand-field effects [30]. In addition, it is expected that the photo-generated electrons from $g-C_3N_4$ can facilitate the conversion of Cu(II) to Cu(I), which is the rate determining step in the catalytic cycle of Cu(II)/Cu(I) for the generation of $\cdot OH$ radicals. The rapid transfer of conduction-band electrons to Cu(II) also could effectively avoid the photogenerated charge recombination [31–33]. Theoretically, this synergistic effect would boost the overall catalytic activity if copper and $(C_{ring})-C_3N_4$ are integrated.

To verify the proposed hypothesis, a series of copper incorporated carbon ring- $g-C_3N_4$ with various copper content were synthesized for H_2O_2 activation under visible light. For comparison, $(C_{ring})-C_3N_4$ and $g-C_3N_4$ were prepared accordingly. MB was selected as a model contaminant to evaluate their photocatalytic activities in the heterogeneous Fenton-like reaction. The main reactive species were identified through specific quenching experiments, and the possible catalytic mechanism was proposed.

2. Materials and methods

2.1. Materials

Melamine, glucose, copper chloride ($CuCl_2 \cdot 2H_2O$), hydrogen peroxide (H_2O_2 , 30 wt%), isopropanol (IPA), ammonium oxalate (AO), diethyldithiocarbamate and sodium hydroxide (NaOH) were purchased from Sinopharm Chemical Reagent Co., Ltd. *p*-benzoquinone (BQ) was supplied by Aladdin Ltd. Methylene blue (MB) and 4-chlorophenol (4-CP) were obtained from Xinzhong Chemical Reagent Co., Ltd. Ethanol (EtOH), hydrochloric acid (HCl) and nitric acid (HNO_3) were acquired from Shanghai Runjie Chemical Reagent Co., Ltd. Silver nitrate ($AgNO_3$) was purchased from Shanghai Chemical Reagent Co. Ltd., China. Coumarin was obtained from Shanghai Macklin Biochemical Co., Ltd. All the chemicals are of analytical grade and used directly.

2.2. Synthesis of copper incorporated carbon ring- $g-C_3N_4$ catalysts

The carbon ring spliced $g-C_3N_4$ (C-CN) was prepared according to a method of Che et al. [13]. The copper incorporated carbon ring- $g-C_3N_4$ (Cu-C-CN) was prepared as follows: Briefly, 5.0 g of melamine and 0.1 g of $CuCl_2$ were consecutively added into 25 mL of $16.0 mg \cdot mL^{-1}$ aqueous solution of glucose under stirring for 1 h, and sonication for 2 h. The mixture was then dried at $60^\circ C$ overnight. The resultant was ground evenly, then calcined at three stages: $300^\circ C$ for 1 h, $400^\circ C$ for 1 h and $550^\circ C$ for 4 h. The obtained powder was washed several times with $0.5 mol \cdot L^{-1}$ HNO_3 and then dried at $80^\circ C$ for 8 h. For comparison, $g-C_3N_4$ (CN) was synthesized by thermal treatment of 5.0 g of melamine under $550^\circ C$ for 4 h. A series of Cu-C-CN were synthesized by adding 0.1 g, 0.2 g, 0.3 g, 0.4 g of $CuCl_2$, and the obtained samples were denoted as 1Cu-C-CN, 2Cu-C-CN, 3Cu-C-CN and 4Cu-C-CN, respectively.

2.3. Characterization methods

The X-ray diffraction (XRD) patterns were recorded on an Ultima IV X-ray diffractometer. Fourier transform infrared (FT-IR) spectra were recorded on a Nicolet iS50 FT-IR spectrophotometer by the method of KBr pellet technique. X-ray photoelectron spectra (XPS) were recorded on a Kratos AXIS Ultra DLD photoelectron spectrometer. The morphology and element mappings were characterized by transmission electron microscopy (TEM, JEM-2100F) and scanning electron microscopy (SEM, S-4800). UV-vis diffuse reflectance spectra (DRS) were measured on a UV-vis-NIR spectrophotometer with the type of Lambda 950. Photoluminescence (PL) spectra were recorded on a Hitachi F-4500 fluorescence spectrophotometer. The total organic carbon (TOC) values were determined using a TOC-L CPN total organic carbon analyzer.

2.4. Catalytic experiments

The catalytic performance of Cu-C-CN catalysts was assessed by the removal of MB in the photo-assisted Fenton-like catalytic process. The initial experimental conditions were as follows: [catalyst] = $0.4 g \cdot L^{-1}$, [MB] = $10 mg \cdot L^{-1}$, [4-CP] = $10 mg \cdot L^{-1}$, [H_2O_2] = $0.10 mol \cdot L^{-1}$, pH₀ = 5.4, visible light ($\lambda > 410 nm$) from a 500 W tungsten lamp. Initially, 20 mg of catalyst was dispersed in 50 mL of MB solution in a photoreactor, which was encircled by the circulating water to ensure a constant temperature. After stirring for 1 h in the dark, H_2O_2 was added and simultaneously the light was turned on to initiate the photo-assisted Fenton-like catalytic process. The sample was collected at certain intervals and then centrifuged. The concentrations of MB were analyzed using a UV-8000 spectrophotometer. Silver nitrate ($AgNO_3$, $0.2 mol \cdot L^{-1}$), isopropanol (IPA, $0.2 mol \cdot L^{-1}$), ammonium oxalate (AO, $0.2 mol \cdot L^{-1}$), or 4-benzoquinone (BQ, $0.2 mol \cdot L^{-1}$) was added into the reaction system to identify the reactive species of $\cdot OH$, h^+ and $O_2^{\cdot -}$, respectively. The stability experiments under the same experiment conditions were conducted as follows: the catalyst was recovered, washed, and dried after each test, then used in the next cycle, until five cycles were conducted. Each test was performed in triplicate.

3. Results and discussion

3.1. Catalysts characterization

The crystallinity of CN, C-CN and Cu-C-CN were characterized by XRD patterns (Fig. 1a). The typical XRD pattern of bulky $g-C_3N_4$ powders have two distinct diffraction peaks located at 27.6° and 12.7° , which can be indexed as (002) and (100) diffraction planes for graphitic materials (JCPDS 87-1526; lattice parameters: $a = b = 4.74 \text{ \AA}$, $c = 6.72 \text{ \AA}$) [34]. The main diffraction peak at 27.6° is a characteristic inter-layer stacking reflection of conjugated aromatic system with an interlayer distance $d = 0.323 nm$, while another peak at 12.7° is

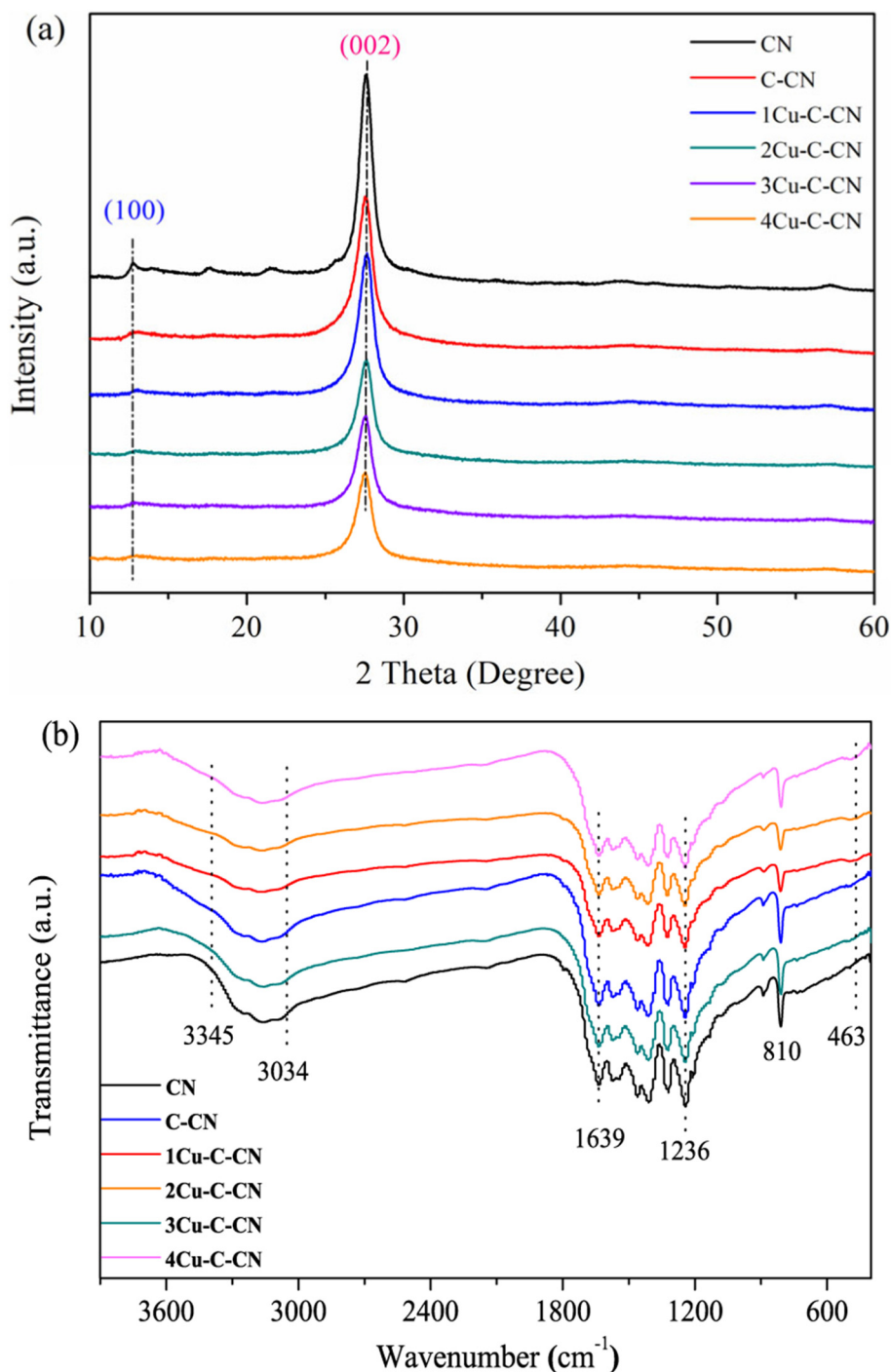


Fig. 1. (a) XRD patterns and (b) FTIR spectra of $g\text{-C}_3\text{N}_4$ (CN), carbon ring spliced $g\text{-C}_3\text{N}_4$ (C-CN), and a series of copper incorporated carbon ring- $g\text{-C}_3\text{N}_4$.

assigned to the in-planar ordering of tri-s-triazine units. As shown in Table S1, 2θ of (002) diffraction peak for all the tested samples varies very slightly ($27.56^\circ\text{--}27.68^\circ$), indicating that C-CN and Cu-C-CN maintain the main structural features of $g\text{-C}_3\text{N}_4$. The corresponding peak intensity decreases after the incorporation of copper and carbon ring, evidencing the successful modification. The average crystallite size (D_{002}) for all the samples were estimated by using the Debye-Scherrer method and full width at half maxima (FWHM) of (002) reflection. The range of average D_{002} is 7.2–8.2 nm (Table S1). Besides, the diffraction peaks ascribed to copper-related compounds are not observed, probably because copper is incorporated at a low concentration or in an amorphous form, or is chemically coordinated to the

matrix of $g\text{-C}_3\text{N}_4$ [35,36].

FTIR spectra of CN, C-CN and Cu-C-CN are displayed in Fig. 1b. As for pristine $g\text{-C}_3\text{N}_4$, the broad absorption bands around 3034 to 3345 cm^{-1} are related to the stretching vibration of N–H bonds and OH bond of absorbed H_2O molecules. The signals at 1236 and 1639 cm^{-1} demonstrate the presence of aromatic C/N heterocycles [37]. The bending vibration of heptazine rings can also be observed at 810 cm^{-1} [38]. The presence of characteristic bands of $g\text{-C}_3\text{N}_4$ in all the samples indicates that the incorporation of copper and carbon ring does not alter the basic CN framework. Regarding to the Cu-C-CN samples, a new peak at 463 cm^{-1} corresponds to the Cu–N bond [39], indicating that the copper species are incorporated into $g\text{-C}_3\text{N}_4$ in the form of

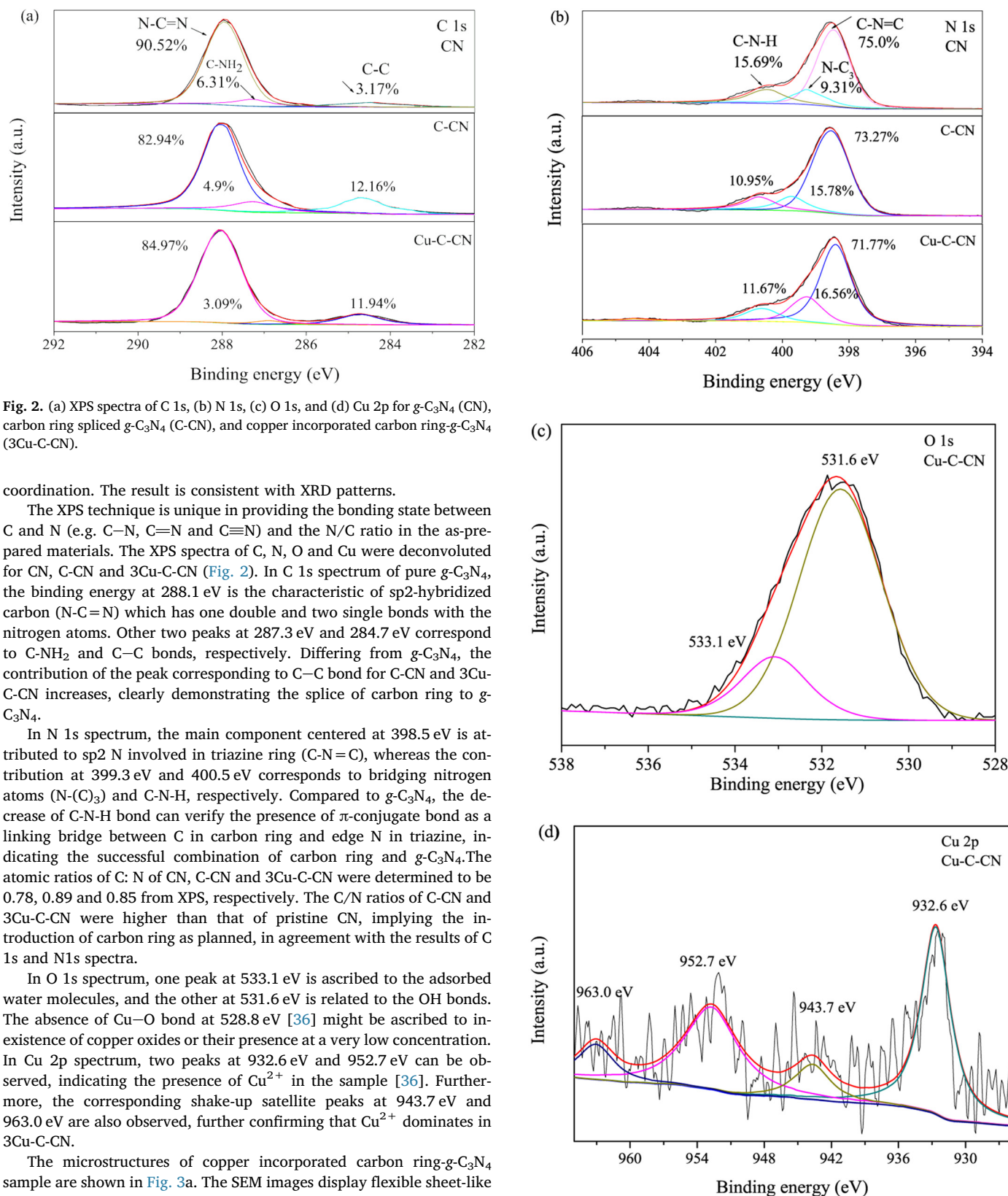


Fig. 2. (a) XPS spectra of C 1s, (b) N 1s, (c) O 1s, and (d) Cu 2p for *g*-C₃N₄ (CN), carbon ring spliced *g*-C₃N₄ (C-CN), and copper incorporated carbon ring-*g*-C₃N₄ (3Cu-C-CN).

coordination. The result is consistent with XRD patterns.

The XPS technique is unique in providing the bonding state between C and N (e.g. C–N, C=N and C≡N) and the N/C ratio in the as-prepared materials. The XPS spectra of C, N, O and Cu were deconvoluted for CN, C-CN and 3Cu-C-CN (Fig. 2). In C 1s spectrum of pure *g*-C₃N₄, the binding energy at 288.1 eV is the characteristic of sp²-hybridized carbon (N-C=N) which has one double and two single bonds with the nitrogen atoms. Other two peaks at 287.3 eV and 284.7 eV correspond to C-NH₂ and C–C bonds, respectively. Differing from *g*-C₃N₄, the contribution of the peak corresponding to C–C bond for C-CN and 3Cu-C-CN increases, clearly demonstrating the splice of carbon ring to *g*-C₃N₄.

In N 1s spectrum, the main component centered at 398.5 eV is attributed to sp² N involved in triazine ring (C-N=C), whereas the contribution at 399.3 eV and 400.5 eV corresponds to bridging nitrogen atoms (N-(C)₃) and C-N-H, respectively. Compared to *g*-C₃N₄, the decrease of C-N-H bond can verify the presence of π-conjugate bond as a linking bridge between C in carbon ring and edge N in triazine, indicating the successful combination of carbon ring and *g*-C₃N₄. The atomic ratios of C: N of CN, C-CN and 3Cu-C-CN were determined to be 0.78, 0.89 and 0.85 from XPS, respectively. The C/N ratios of C-CN and 3Cu-C-CN were higher than that of pristine CN, implying the introduction of carbon ring as planned, in agreement with the results of C 1s and N1s spectra.

In O 1s spectrum, one peak at 533.1 eV is ascribed to the adsorbed water molecules, and the other at 531.6 eV is related to the OH bonds. The absence of Cu–O bond at 528.8 eV [36] might be ascribed to inexistence of copper oxides or their presence at a very low concentration. In Cu 2p spectrum, two peaks at 932.6 eV and 952.7 eV can be observed, indicating the presence of Cu²⁺ in the sample [36]. Furthermore, the corresponding shake-up satellite peaks at 943.7 eV and 963.0 eV are also observed, further confirming that Cu²⁺ dominates in 3Cu-C-CN.

The microstructures of copper incorporated carbon ring-*g*-C₃N₄ sample are shown in Fig. 3a. The SEM images display flexible sheet-like morphology and smooth surface without nanoparticles decorated on it. Furthermore, the edges of the nanosheets spontaneously curl due to the ultrathin feature. SEM elemental mappings (Fig. 3b) show that the existence of C, N, O and Cu elements in 3Cu-C-CN sample and they are uniformly distributed on its surface. C signals are observable in the marked elliptic regions. These abundant C signals can be assigned to the presence of in-plane carbon ring, due to the absence of carbon dots or

other carbon impurity.

As displayed in the TEM image of 3Cu-C-CN (Fig. S1a), a smooth surface is observed without obvious nanoparticles or crystallite structure of copper species dispersed on it, indicating that the copper species

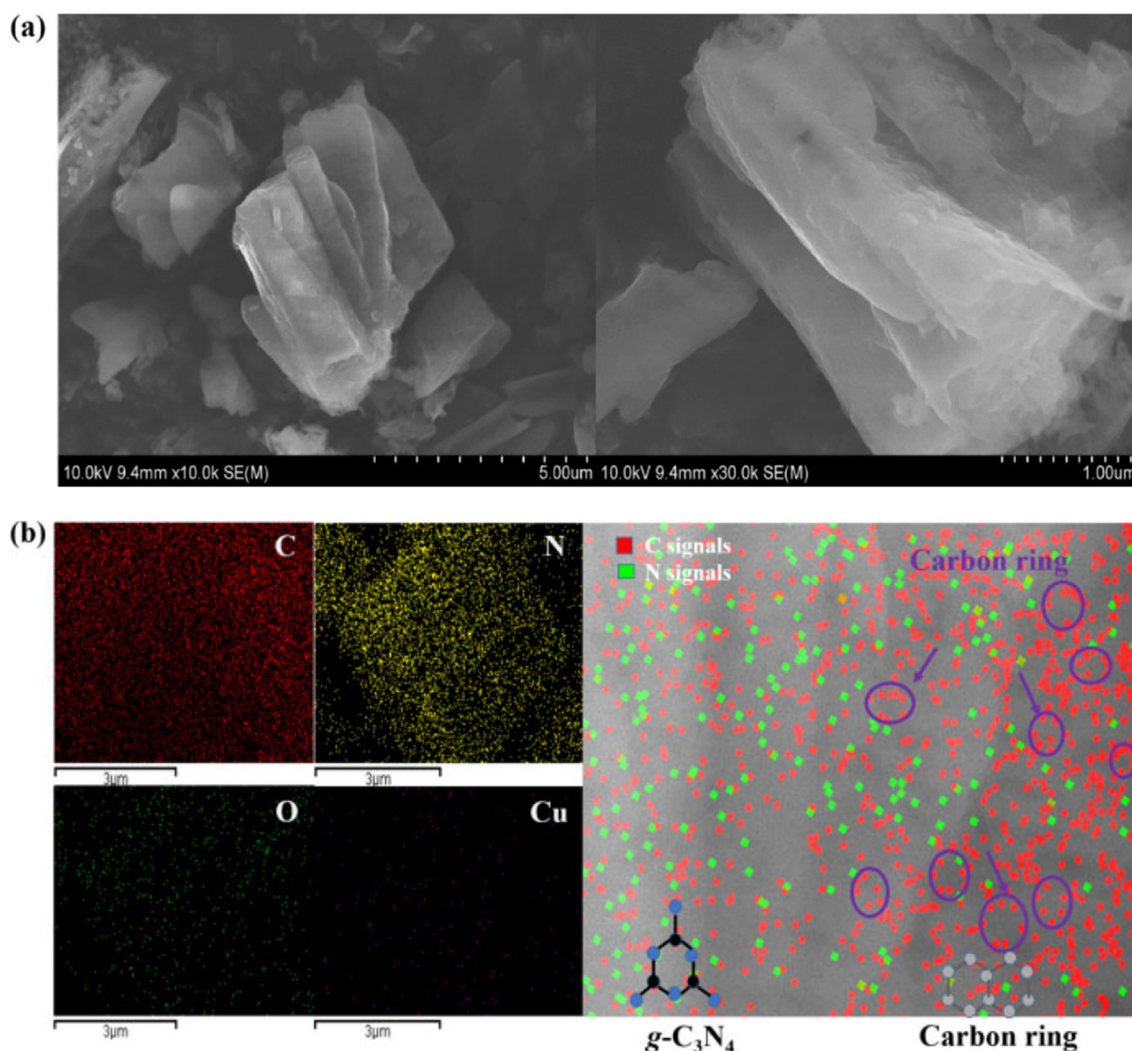


Fig. 3. (a) SEM images and (b) element mappings of 3Cu-C-CN.

may exist in the framework of $g\text{-C}_3\text{N}_4$ in the form of Cu^{2+} , consistent with the results of XRD, FTIR and XPS. As illustrated in Fig. S1b, two different lattice fringes of 0.21 nm and 0.24 nm are present, which can be assigned to the (100) planes of graphite and in-plane d -spacing distance in $g\text{-C}_3\text{N}_4$ [13], respectively.

The optical property of all samples is shown in Fig. 4a. The splice of carbon ring obviously enhances the visible-light absorption ability of $g\text{-C}_3\text{N}_4$ in the region of 450–800 nm, which can promote utilization of the low-energy visible light. Once copper is incorporated, the enhanced visible-light absorption in 450–800 nm can be also observed. With the increase in copper content, the ability to absorb visible light gradually increases. The result reveals that the copper species are successfully incorporated into the framework of $g\text{-C}_3\text{N}_4$ [40]. Additionally, absorption band of C-CN as well as Cu-C-CN exhibit apparent red shift compared to pure $g\text{-C}_3\text{N}_4$, which can accelerate the generation of photo-induced carriers under visible light irradiation, thus resulting in the enhanced photocatalytic properties [41].

Photoluminescence (PL) spectra were measured to comprehend the transfer and recombination behaviors of photo-generated charge carriers in copper incorporated carbon ring- $g\text{-C}_3\text{N}_4$ samples. In general, the weaker of PL intensity, the higher separation efficiency of carriers. As depicted in Fig. 4b, pristine $g\text{-C}_3\text{N}_4$ exhibits the strongest photoluminescence with an emission peak around 470 nm. This strong peak is attributed to the band-band PL phenomenon with the energy of light roughly equal to the band gap energy of $g\text{-C}_3\text{N}_4$ (2.7 eV). However, the

PL intensity is apparently decreased after the splice of carbon ring, verifying that the carbon ring can capture the photo-generated electrons to significantly diminish the recombination rate of charge carriers. Moreover, the PL intensity sharply decreased after the incorporation of copper species on carbon ring spliced $g\text{-C}_3\text{N}_4$ (C-CN), and the increase of copper content can further inhibit the combination of photo-generated charges. The results adequately confirm that the copper and carbon contents greatly affect the recombination rate of charge carriers. Therefore, the expedited charge separation is desirable for the photocatalytic reactions, as verified later.

3.2. Catalytic performance

The catalytic activities of as-prepared catalysts were evaluated by testing the degradation rates of MB in the photo-assisted Fenton-like catalytic process. For comparison, the photocatalytic processes were conducted under visible light irradiation. The Fenton-like processes were carried out in the dark in the presence of H_2O_2 .

As shown in Fig. 5a, the MB concentration has no apparent change when only H_2O_2 and visible light are employed without catalysts. Compared to pure $g\text{-C}_3\text{N}_4$, the degradation efficiency of MB increases in the presence of C-CN in the photo-assisted Fenton-like catalytic process, indicating that carbon ring doped $g\text{-C}_3\text{N}_4$ can separate photogenerated charges effectively for the improvement of catalytic activity. However, the catalytic performance is significantly enhanced with further

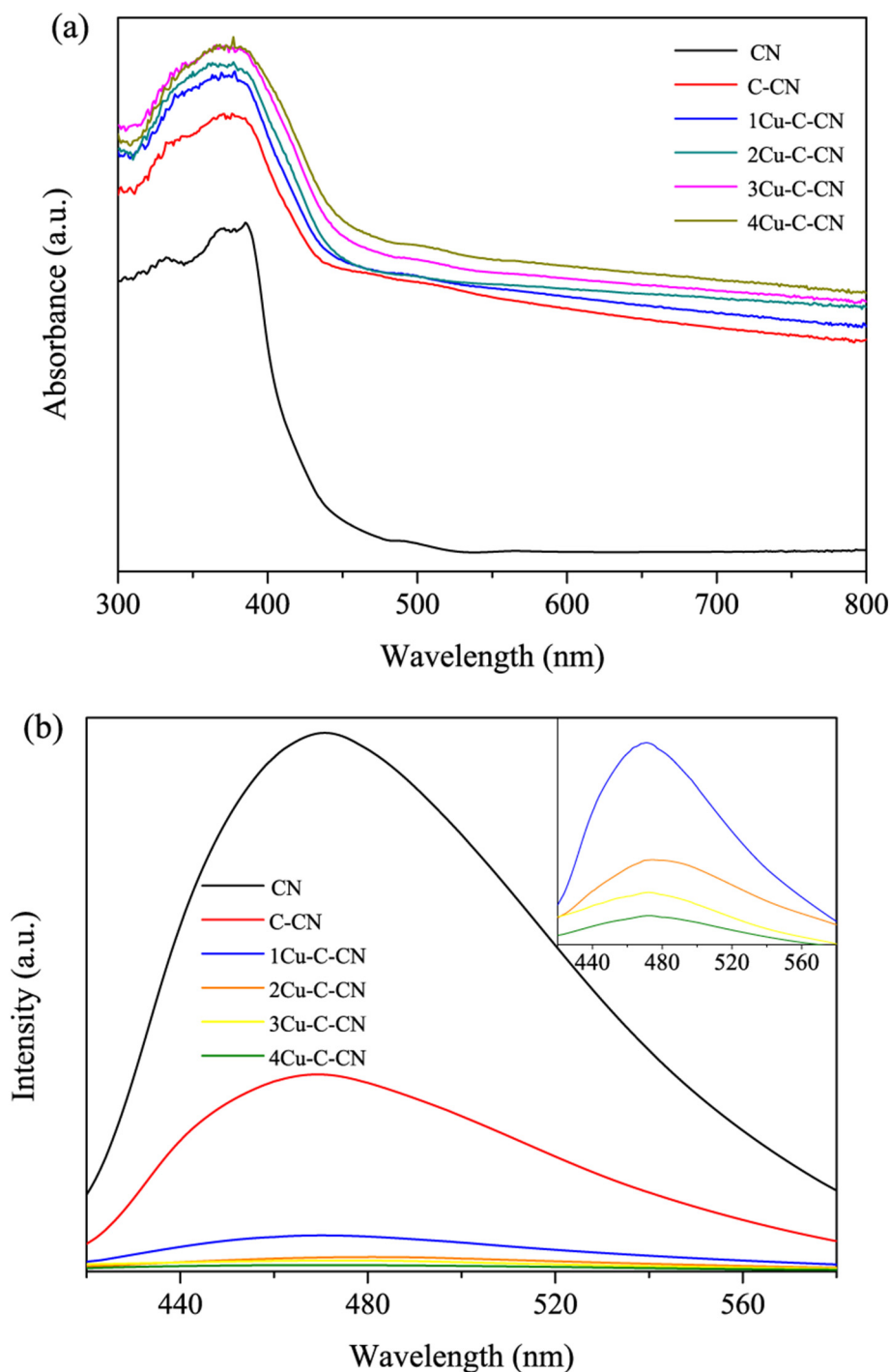


Fig. 4. (a) UV-vis diffuse reflectance spectra and (b) PL spectra of $g\text{-C}_3\text{N}_4$ (CN), carbon ring spliced $g\text{-C}_3\text{N}_4$ (C-CN), and copper incorporated carbon ring- $g\text{-C}_3\text{N}_4$ (Cu-C-CN). (Excitation wavelength at 365 nm).

introduction of copper species, demonstrating that the copper species play an important role in MB degradation as copper species can activate H_2O_2 to generate hydroxyl radicals. In particular, 3Cu-C-CN catalyst displays the best catalytic activity. Further increasing the copper content can reduce the catalytic performance, because excess copper species may serve as recombination centers for electron-hole pairs [41,42].

To quantitatively analyze the catalytic performance of different catalysts for MB degradation, the reaction rate constants (k) obtained through the Langmuir-Hinshelwood kinetics model are exhibited in a column chart in Fig. 5b. Briefly, for each tested material, degradation performance of the photo-assisted Fenton-like catalytic processes is

superior to those of separate photocatalytic processes and Fenton-like catalytic processes. For example, the kinetic constant for 3Cu-C-CN in the photo-assisted Fenton-like catalytic process is about 5.5 times higher than that of pure $g\text{-C}_3\text{N}_4$. Additionally, the kinetic constant for each catalyst in the photo-assisted Fenton-like catalytic processes is greater than the sum of its rate constant in the corresponding photocatalytic processes and Fenton-like processes, especially at a higher Cu loading. For instance, the rate constant of the photo-assisted Fenton-like catalytic processes is $176.4 \times 10^{-4} \text{ min}^{-1}$ for 3Cu-C-CN, much larger than the sum of the corresponding photocatalytic process ($10.1 \times 10^{-4} \text{ min}^{-1}$) and Fenton-like process ($36.1 \times 10^{-4} \text{ min}^{-1}$).

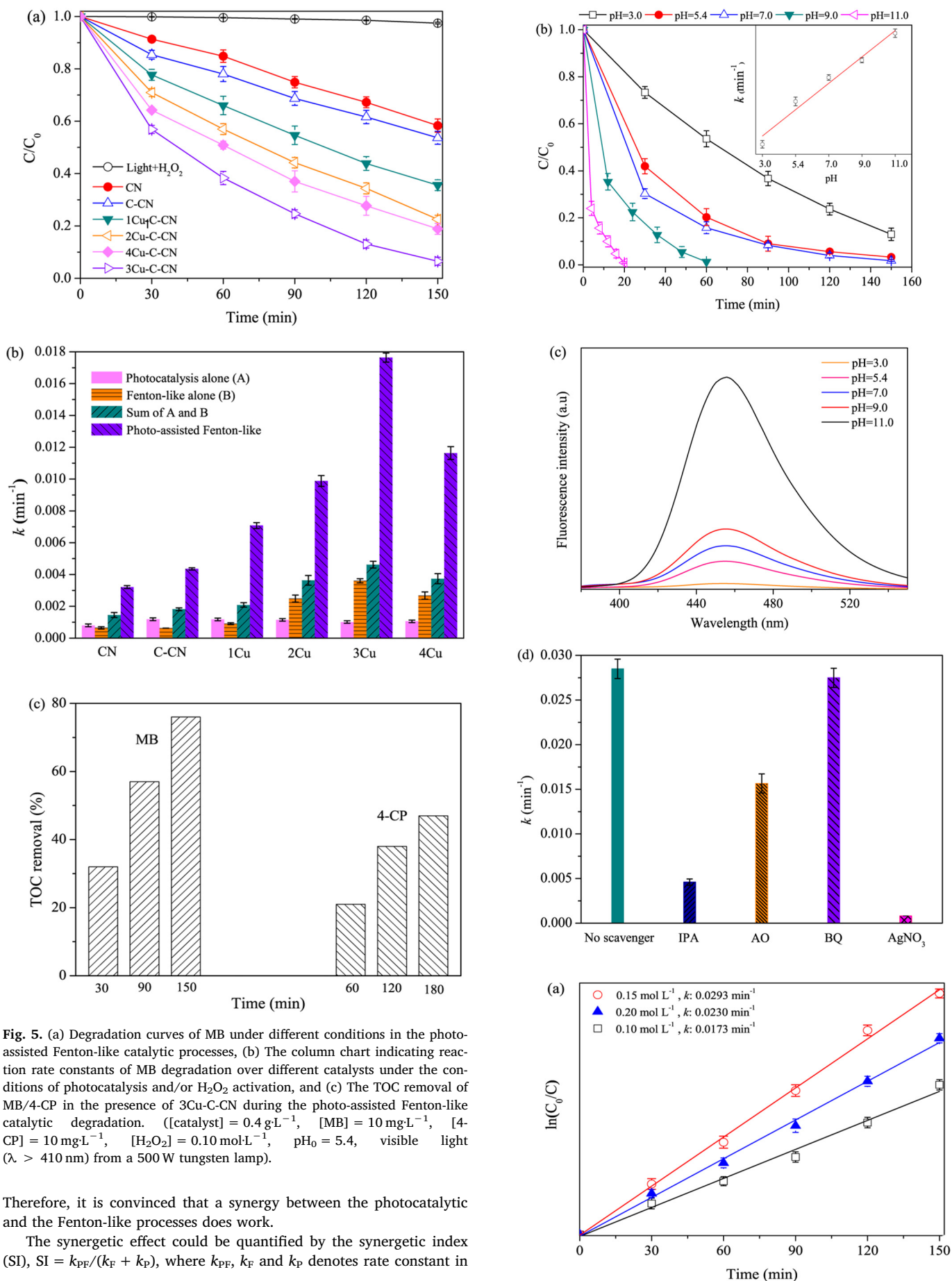


Fig. 5. (a) Degradation curves of MB under different conditions in the photo-assisted Fenton-like catalytic processes, (b) The column chart indicating reaction rate constants of MB degradation over different catalysts under the conditions of photocatalysis and/or H₂O₂ activation, and (c) The TOC removal of MB/4-CP in the presence of 3Cu₄C-CN during the photo-assisted Fenton-like catalytic degradation. ([catalyst] = 0.4 g·L⁻¹, [MB] = 10 mg·L⁻¹, [4-CP] = 10 mg·L⁻¹, [H₂O₂] = 0.10 mol·L⁻¹, pH₀ = 5.4, visible light (λ > 410 nm) from a 500 W tungsten lamp).

Therefore, it is convinced that a synergy between the photocatalytic and the Fenton-like processes does work.

The synergetic effect could be quantified by the synergetic index (SI), SI = k_{PF}/(k_F + k_P), where k_{PF}, k_F and k_P denotes rate constant in

Fig. 6. (a) The curves of $\ln(C_0/C)$ versus Time under different H_2O_2 concentration. ([catalyst] = $0.4 \text{ g}\cdot\text{L}^{-1}$, [MB] = $10 \text{ mg}\cdot\text{L}^{-1}$, $\text{pH}_0 = 5.4$), (b) Effect of initial pH on MB degradation using 3Cu-C-CN as the catalyst. ([catalyst] = $0.4 \text{ g}\cdot\text{L}^{-1}$, [MB] = $10 \text{ mg}\cdot\text{L}^{-1}$, $[H_2O_2] = 0.10 \text{ mol}\cdot\text{L}^{-1}$), (c) Fluorescence intensity of 7-hydroxycoumarin after reaction in the system of 3Cu-C-CN- H_2O_2 -coumarin. ([catalyst] = $0.4 \text{ g}\cdot\text{L}^{-1}$, $[H_2O_2] = 0.10 \text{ mol}\cdot\text{L}^{-1}$, [coumarin] = $1.0 \text{ mol}\cdot\text{L}^{-1}$, fluorescence reaction time = 150 min), and (d) The effect of different scavengers on MB degradation over 3Cu-C-CN in the photo-assisted Fenton-like catalytic processes. ([catalyst] = $0.4 \text{ g}\cdot\text{L}^{-1}$, [MB] = $10 \text{ mg}\cdot\text{L}^{-1}$, $[H_2O_2] = 0.15 \text{ mol}\cdot\text{L}^{-1}$, $\text{pH}_0 = 5.4$).

photo-assisted Fenton-like catalytic processes, Fenton-like catalytic processes and photocatalytic processes, respectively. Gong et al. [29] synthesized the MOF-derived nitrogen doped carbon modified $g\text{-C}_3\text{N}_4$ (ZIF-NC/ $g\text{-C}_3\text{N}_4$) heterostructure composite to degrade bisphenol A (BPA) with peroxydisulfate under visible light irradiation. The estimated SI for 0.5% ZIF-NC/ $g\text{-C}_3\text{N}_4$ was 1.15. Li et al. [15] prepared $g\text{-C}_3\text{N}_4/\text{NH}_2$ -iron terephthalate metal-organic framework (Ip-x) for MB degradation in the visible light-induced Fenton-like process. The SI of the Ip-2/visible light/ H_2O_2 system was calculated to be 4.05. Ai et al. [43] applied iron terephthalate metal-organic framework MIL-53(Fe) to oxidize RhB, the value of SI being calculated as 2.22. The obtained SI for 3Cu-C-CN is 3.82, larger than that for CN (2.21) and C-CN (2.39). The substantial synergistic effect for 3Cu-C-CN demonstrates the importance of perfect incorporation of copper and carbon ring in separation of photogenerated electron-hole pairs and regeneration of catalyst (i.e. Cu^+ ions).

The mineralization of organics is always expected in the treatment of organic pollutants. Total organic carbon (TOC) is an indicator, which can be used to assess the mineralization degree of organics. Herein, MB and 4-CP are used as the substrates to evaluate the TOC removal efficiency over 3Cu-C-CN under the same conditions (Fig. 5c). With the increase of reaction time, the TOC value gradually decreases. It finally achieves 76% or 47% removal after 150 min or 180 min, indicating that 3Cu-C-CN can efficiently mineralize MB/4-CP. Contrastively, only 41.5% of BPA over CN-Cu(II)- $\text{CuAlO}_2\text{-H}_2\text{O}_2$ [44] or 57% of MB over Ti/ $\text{CuO-H}_2\text{O}_2$ [45] can be mineralized, indicating that 3Cu-C-CN can be a feasible catalyst for organic degradation.

The effect of H_2O_2 concentration on MB degradation was explored using 3Cu-C-CN as the catalyst in the photo-assisted Fenton-like processes. The rate constants were obtained by the slope of the $\ln(C_0/C)$ vs. time plot, as depicted in Fig. 6a. The corresponding k value at various H_2O_2 concentration of $0.10 \text{ mol}\cdot\text{L}^{-1}$, $0.15 \text{ mol}\cdot\text{L}^{-1}$ and $0.20 \text{ mol}\cdot\text{L}^{-1}$ are

0.0173 ($R^2 = 0.988$), 0.0293 ($R^2 = 0.996$), and 0.0230 min^{-1} ($R^2 = 0.995$), respectively. This can be due to the dual roles of H_2O_2 in $\cdot\text{OH}$ generation. With increasing the H_2O_2 concentration, the k value increases and more hydroxyl radicals can be yielded for MB removal. However, at a higher concentration, the k value decreases and the degradation efficiency is decreased due to the scavenging effect of $\cdot\text{OH}$ by excessive H_2O_2 to generate $\text{HO}_2\cdot$ with lower oxidation potential [46,47]. Therefore, a suitable concentration of H_2O_2 is required.

The pH value is often considered to be a sensitive factor in Fenton reaction, thus the influence of initial pH value on the degradation of MB over 3Cu-C-CN was also investigated in the photo-assisted Fenton-like catalytic process (Fig. 6b). It can be clearly seen that the degradation efficiency is greatly enhanced as the pH value increases. In general, the values of k nearly linearly increase with pH ($R^2 = 0.964$). At pH 3.0, about 86% of degradation is achieved in 150 min, and when increasing the pH value to 11.0, 99.2% of removal is obtained within 20 min. This may be due to the increase of reactive radicals at higher pH values. At a lower pH, more H^+ ions are generated that can scavenge $\cdot\text{OH}$ ($\cdot\text{OH} + \text{H}^+ + e^- \rightarrow \text{H}_2\text{O}$), leading to a decrease in degradation efficiency [48]. Under alkaline conditions, it is HO_2^- anions not H_2O_2 that plays the main role, which can be further oxidized to $\text{O}_2\cdot^-$ and other reactive species by holes generated in 3Cu-C-CN during the photo-assisted Fenton-like catalytic processes, besides high level of OH^- can also be oxidized by h^+ , facilitating the generation of $\cdot\text{OH}$ [49,50]. Since $\cdot\text{OH}$ are the primary reactive species in the photo-assisted Fenton-like catalytic process, as demonstrated in Fig. 6d, thus the degradation of MB is accelerated at higher pH values.

The non-fluorescent coumarin was used to identify the generated $\cdot\text{OH}$, which can produce high-fluorescent 7-hydroxycoumarin [51]. As expected, an increasing fluorescence intensity is observed when pH increases (Fig. 6c), in consistent with the pH dependence of MB degradation. Furthermore, the stability tests of MB in the presence of H_2O_2 under different pH values were also conducted (Fig. S2). MB is relatively stable in the presence of H_2O_2 at various pH value. Therefore, the enhanced removal of MB at alkaline pH is ascribed to photo-degradation by Cu-C-CN/ H_2O_2 , rather than its self-decomposition under alkaline conditions.

In Fig. 6d, to identify other main reactive species, BQ, AO, IPA or AgNO_3 was selected as a scavenger for $\text{O}_2\cdot^-$, h^+ , $\cdot\text{OH}$ or e^- , respectively [52]. The addition of BQ has a negligible influence on MB degradation, suggesting that contribution of $\text{O}_2\cdot^-$ is insignificant in the overall photo-assisted Fenton-like catalytic process. While AO is added,

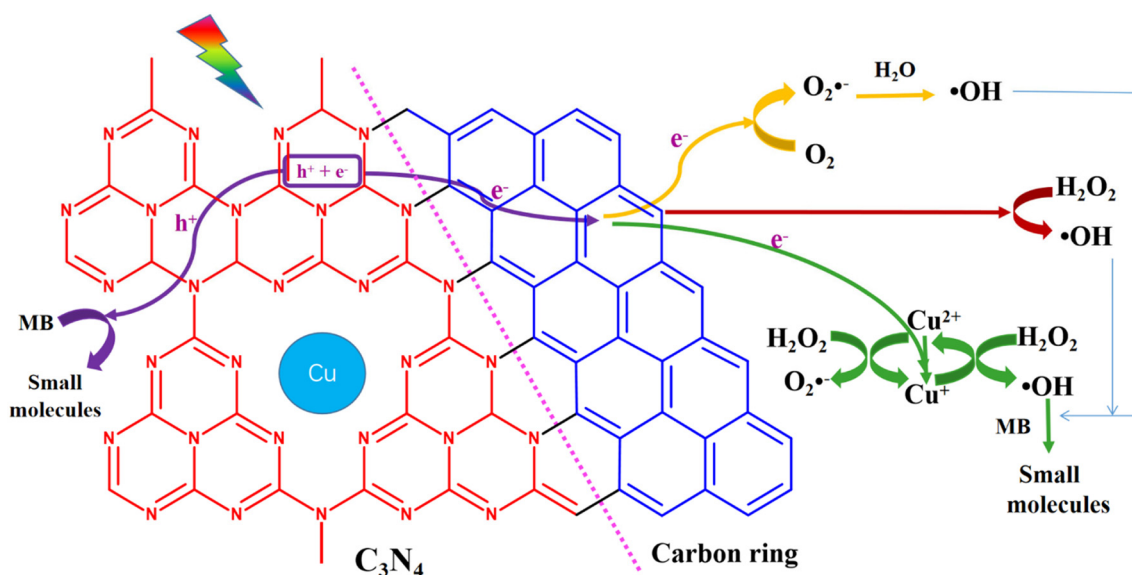


Fig. 7. Photo-assisted Fenton-like catalytic degradation mechanism of copper incorporated carbon ring- $g\text{-C}_3\text{N}_4$.

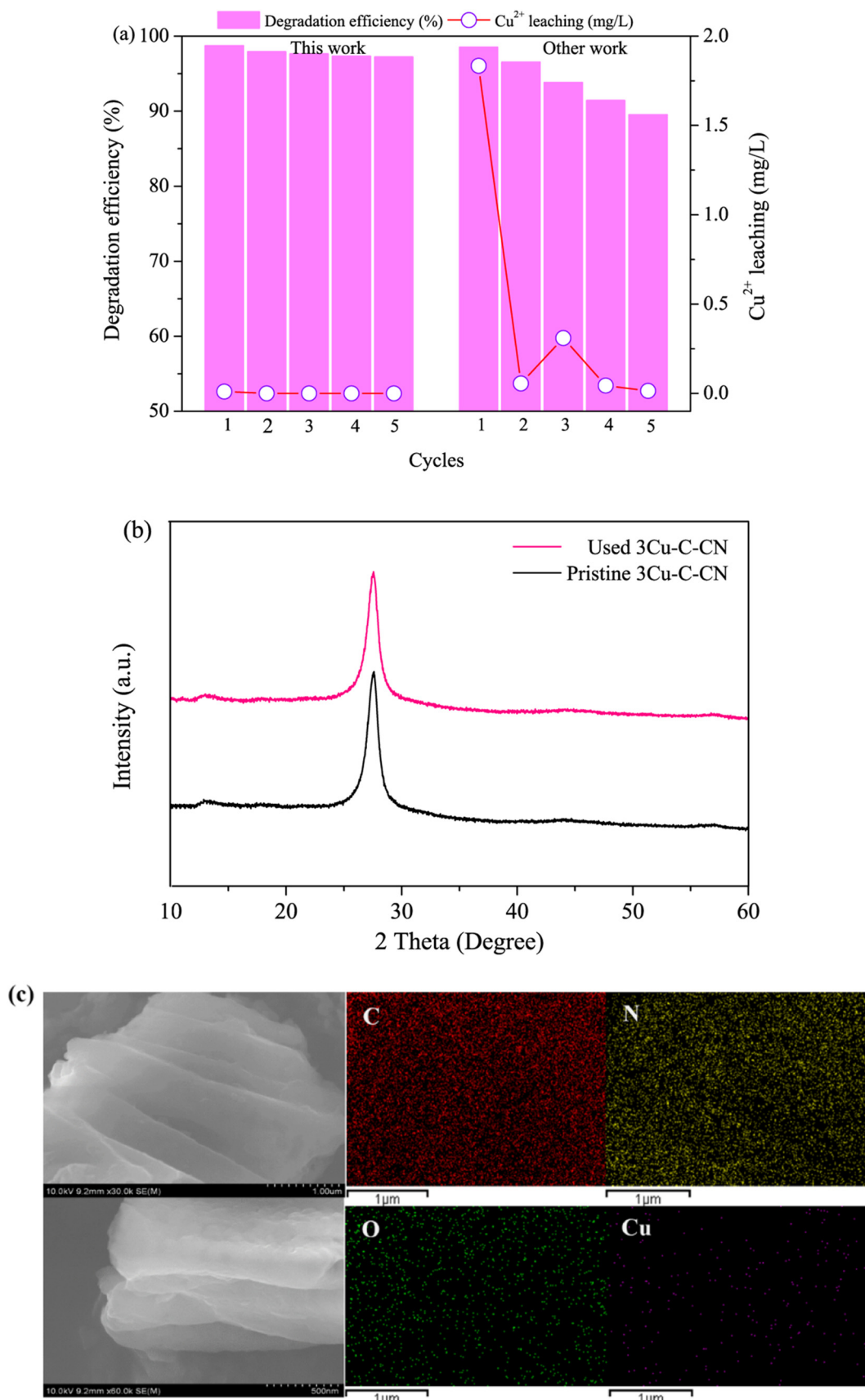
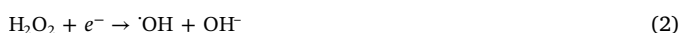


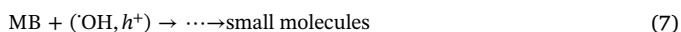
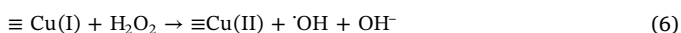
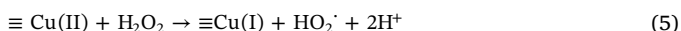
Fig. 8. (a) The MB degradation efficiency and Cu²⁺ leaching concentration in the photo-assisted Fenton-like catalytic processes over 3Cu-C-CN for five cycles. ([catalyst] = 0.4 g·L⁻¹, [MB] = 10 mg·L⁻¹, [H₂O₂] = 0.15 mol·L⁻¹, pH₀ = 5.4, [diethyldithiocarbamate] = 54 mg·L⁻¹), (b) Comparison of XRD patterns, and (c) SEM images and element mappings after five cycles.

the degradation rate of MB is halved, indicating that h^+ plays a role in this catalytic degradation process. $\cdot\text{OH}$ radicals should be the primary reactive species because of a significant influence of IPA on MB removal. However, as AgNO_3 is present, the degradation of MB is nearly completely inhibited. This result indicates those electron-driven Cu(II)/Cu(I) redox cycling (Eq. (1)) and H_2O_2 activation (Eq. (2)) may be critical for the enhanced degradation performance.



3.3. Catalytic mechanism

A possible photo-assisted Fenton-like catalytic mechanism for pollutant degradation over copper incorporated carbon ring- $g\text{-C}_3\text{N}_4$ composite is illustrated in Fig. 7. Under visible light irradiation, electrons are excited to the CB of $g\text{-C}_3\text{N}_4$ while holes remain in its VB (Reaction 3). The excited electrons can further transfer to the surface of electron-deficient carbon ring, achieving the effective separation of photo-generated carriers. As manifested in the radical scavenging experiments, the survived electrons are vital for the overall catalytic degradation of MB because 1) they can react with dissolved oxygen to yield $\text{O}_2^{\cdot-}$, further combining with H_2O_2 to produce $\cdot\text{OH}$ (Reaction 4) [53,54]. The holes left on VB of $g\text{-C}_3\text{N}_4$ can directly oxidize MB [55]; 2) they can directly reduce H_2O_2 to form $\cdot\text{OH}$ (Reaction 2); and they can promote the conversion of Cu(II) to Cu(I) (0.16 V, vs SHE) (Reaction 1) [56], thus accelerating the production of reactive hydroxyl radicals. In addition, Cu(II) can also be reduced to Cu(I) by the reaction with H_2O_2 (Reaction 5), meanwhile the generated Cu(I) can react with H_2O_2 , accompanying the generation of $\cdot\text{OH}$ radicals (Reaction 6). Therefore, the processes as described in Reactions 1–6 display a synergistic effect between the photocatalytic and Fenton-like processes. The rapid trap of conduction-band electrons by Cu(II) not only expedites the rate determining step ($\text{Cu(II)} \rightarrow \text{Cu(I)}$) in the Fenton-like reactions, but also effectively minimizes the charge recombination. This kind of “Two Birds One Stone” synergy can facilitate the generation of $\cdot\text{OH}$. In this system, the generated reactive species, including h^+ and $\cdot\text{OH}$ radicals, can attack MB molecules which are finally mineralized into small molecules (Reaction 7).



3.4. Stability of copper incorporated carbon ring- $g\text{-C}_3\text{N}_4$

The stability of a catalyst is an important index to evaluate the feasibility of the catalyst. To assess the catalytic reusability of Cu-C-CN composite on MB degradation, the catalyst was recovered to conduct five consecutive cycles in the photo-assisted Fenton-like catalytic process, and the results are displayed in Fig. 8a. The concentration of leached Cu^{2+} ions after each cycle was detected using the method of chromogenic reaction, where diethyldithiocarbamate was used as the chromogenic agent for Cu^{2+} . In the photo-assisted Fenton-like catalytic processes, the maximum concentration of leached Cu^{2+} is $0.0105 \text{ mg}\cdot\text{L}^{-1}$, much lower than that of the European Union directives ($< 2.0 \text{ mg}\cdot\text{L}^{-1}$) and United States regulations ($< 1.3 \text{ mg}\cdot\text{L}^{-1}$) [44]. Clearly, Cu^{2+} is hardly leached after the second cycle and the degradation efficiency retains almost unchanged, which validates that Cu-C-CN can be a feasible Fenton catalyst with good stability and durability for H_2O_2 activation to degrade MB. The spliced carbon ring to

C_3N_4 with different electron affinity probably yields a strong in-building electric field in Cu-C-CN , solidifying the stability of Cu in Cu-C-CN . For comparison, the degradation efficiency and Cu^{2+} leaching in previous reports [57] are also illustrated. Obviously, both stability and reusability of 3Cu-C-CN are superior to the reported catalysts, as shown in Fig. 8a and Fig. S3. To further demonstrate the stability of 3Cu-C-CN , the catalyst after five cycles was measured by XRD pattern (Fig. 8b) and SEM (Fig. 8c). Expectedly, the diffraction peak do not change greatly after five runs and the morphology retains sheet-like. The results indicate that Cu-C-CN is an applicable catalyst with excellent stability.

4. Conclusions

In this study, copper incorporated carbon ring- $g\text{-C}_3\text{N}_4$ catalysts have been developed via a facile calcination method. The catalyst was characterized by XRD, FT-IR, XPS, TEM, SEM, UV-vis DRS and PL. The as-prepared 3Cu-C-CN catalyst attains the best catalytic performance toward the removal of MB in comparison with pure $g\text{-C}_3\text{N}_4$. The splice of carbon ring with $g\text{-C}_3\text{N}_4$ can benefit the effective separation of charge carriers. Owing to the rapid transfer of photogenerated electrons to Cu(II) sites, the redox cycling of Cu(II)/Cu(I) is accelerated, leading to efficient activation of H_2O_2 and therefore promoting the MB degradation based on hydroxyl radicals. Importantly, the synergistic effects between photocatalytic and Fenton-like process facilitate the generation of reactive radicals, such as holes and hydroxyl radicals, as evidenced by radicals scavenging tests and specific fluorescent probe reaction for $\cdot\text{OH}$. The very low copper leaching of 3Cu-C-CN suggests its excellent recycling stability. Therefore, the copper incorporated carbon ring- $g\text{-C}_3\text{N}_4$ can serve as an efficient and stable catalyst for wastewater treatment.

Declaration of Competing Interest

There are no conflicts of interest to declare.

Acknowledgements

This work was partly supported by Research Start-Up Fund for New Staff (Z.W). The authors thank Mr. Bo Sheng from Donghua University for his assistance in manuscript revision.

Appendix A. Supplementary data

Supplementary data to this article can be found online at <https://doi.org/10.1016/j.apsusc.2019.05.288>.

References

- [1] X. Wang, K. Maeda, A. Thomas, K. Takanebe, G. Xin, J.M. Carlsson, K. Domen, M. Antonietti, A metal-free polymeric photocatalyst for hydrogen production from water under visible light, *Nat. Mater.* 8 (2009) 76–80.
- [2] X. Yuan, C. Zhou, Y. Jin, Q. Jing, Y. Yang, X. Shen, Q. Tang, Y. Mu, A.K. Du, Facile synthesis of 3D porous thermally exfoliated $g\text{-C}_3\text{N}_4$ nanosheet with enhanced photocatalytic degradation of organic dye, *J. Colloid Interface Sci.* 468 (2016) 211–219.
- [3] X. Liu, H. Ji, J. Wang, J. Xiao, H. Yuan, D. Xiao, Ozone treatment of graphitic carbon nitride with enhanced photocatalytic activity under visible light irradiation, *J. Colloid Interface Sci.* 505 (2017) 919–928.
- [4] W.-J. Ong, L.-L. Tan, Y.H. Ng, S.-T. Yong, S.-P. Chai, Graphitic carbon nitride ($g\text{-C}_3\text{N}_4$)-based photocatalysts for artificial photosynthesis and environmental remediation: are we a step closer to achieving sustainability? *Chem. Rev.* 116 (2016) 7159–7329.
- [5] J. Wen, J. Xie, X. Chen, X. Li, A review on $g\text{-C}_3\text{N}_4$ -based photocatalysts, *Appl. Surf. Sci.* 391 (2017) 72–123.
- [6] E. Liu, J. Chen, Y. Ma, J. Feng, J. Jia, J. Fan, X. Hu, Fabrication of 2D $\text{SnS}_2/g\text{-C}_3\text{N}_4$ heterojunction with enhanced H_2 evolution during photocatalytic water splitting, *J. Colloid Interface Sci.* 524 (2018) 313–324.
- [7] Y.-P. Zhu, M. Li, Y.-L. Liu, T.-Z. Ren, Z.-Y. Yuan, Carbon-doped ZnO hybridized homogeneously with graphitic carbon nitride nanocomposites for photocatalysis, *J. Phys. Chem. C* 118 (2014) 10963–10971.
- [8] S. Zhao, J. Liu, C. Li, W. Ji, M. Yang, H. Huang, Y. Liu, Z. Kang, Tunable ternary (N,

- P, B)-doped porous nanocarbons and their catalytic properties for oxygen reduction reaction, *ACS Appl. Mater. Interfaces* 6 (2014) 22297–22304.
- [9] L. Liu, Y. Qi, J. Hu, Y. Liang, W. Cui, Efficient visible-light photocatalytic hydrogen evolution and enhanced photostability of core/shell $\text{Cu}_2\text{O}@g\text{-C}_3\text{N}_4$ octahedra, *Appl. Surf. Sci.* 351 (2015) 1146–1154.
- [10] M.Q. Wen, T. Xiong, Z.G. Zang, W. Wei, X.S. Tang, F. Dong, Synthesis of $\text{MoS}_2/g\text{-C}_3\text{N}_4$ nanocomposites with enhanced visible-light photocatalytic activity for the removal of nitric oxide (NO), *Opt. Express* 24 (2016) 10205–10212.
- [11] Y.P. Zhu, T.Z. Ren, Z.Y. Yuan, Mesoporous phosphorus-doped $g\text{-C}_3\text{N}_4$ nanostructured flowers with superior photocatalytic hydrogen evolution performance, *ACS Appl. Mater. Interfaces* 7 (2015) 16850–16856.
- [12] J. Li, B. Shen, Z. Hong, B. Lin, B. Gao, Y. Chen, A facile approach to synthesize novel oxygen-doped $g\text{-C}_3\text{N}_4$ with superior visible-light photoreactivity, *Chem. Commun.* 48 (2012) 12017–12019.
- [13] W. Che, W. Cheng, T. Yao, F. Tang, W. Liu, H. Su, Y. Huang, Q. Liu, J. Liu, F. Hu, Z. Pan, Z. Sun, S. Wei, Fast photoelectron transfer in $(\text{C}_{\text{ring}})\text{-C}_3\text{N}_4$ plane heterostructural nanosheets for overall water splitting, *J. Am. Chem. Soc.* 139 (2017) 3021–3026.
- [14] D.H. Bremner, R. Molina, F. Martínez, J.A. Melero, Y. Segura, Degradation of phenolic aqueous solutions by high frequency sono-Fenton systems ($\text{US-Fe}_2\text{O}_3/\text{SBA-15-H}_2\text{O}_2$), *Appl. Catal. B Environ.* 90 (2009) 380–388.
- [15] X. Li, Y. Pi, L. Wu, Q. Xia, J. Wu, Z. Li, J. Xiao, Facilitation of the visible light-induced Fenton-like excitation of H_2O_2 via heterojunction of $g\text{-C}_3\text{N}_4/\text{NH}_2\text{-Iron terephthalate metal-organic framework for MB degradation}$, *Appl. Catal. B Environ.* 202 (2017) 653–663.
- [16] F. Chai, K. Li, C. Song, X. Guo, Synthesis of magnetic porous $\text{Fe}_3\text{O}_4/\text{C}/\text{Cu}_2\text{O}$ composite as an excellent photo-Fenton catalyst under neutral condition, *J. Colloid Interface Sci.* 475 (2016) 119–125.
- [17] H.Y. Xu, B. Li, T.N. Shi, Y. Wang, S. Komarneni, Nanoparticles of magnetite anchored onto few-layer graphene: a highly efficient Fenton-like nanocomposite catalyst, *J. Colloid Interface Sci.* 532 (2018) 161–170.
- [18] D.A. Nichela, A.M. Berkovic, M.R. Costante, M.P. Juliarena, F.S. García Einschlag, Nitrobenzene degradation in Fenton-like systems using Cu(II) as catalyst. Comparison between Cu(II)- and Fe(III)-based systems, *Chem. Eng. J.* 228 (2013) 1148–1157.
- [19] Y. Diao, Z. Yan, M. Guo, X. Wang, Magnetic multi-metal co-doped magnesium ferrite nanoparticles: an efficient visible light-assisted heterogeneous Fenton-like catalyst synthesized from saprolite laterite ore, *J. Hazard. Mater.* 344 (2018) 829–838.
- [20] L. Zhang, Y. Nie, C. Hu, X. Hu, Decolorization of methylene blue in layered manganese oxide suspension with H_2O_2 , *J. Hazard. Mater.* 190 (2011) 780–785.
- [21] S. Karthikeyan, R. Boopathy, G. Sekaran, In situ generation of hydroxyl radical by cobalt oxide supported porous carbon enhance removal of refractory organics in tannery dyeing wastewater, *J. Colloid Interface Sci.* 448 (2015) 163–174.
- [22] Z. Li, J. Lyu, M. Ge, Synthesis of magnetic $\text{Cu}/\text{CuFe}_2\text{O}_4$ nanocomposite as a highly efficient Fenton-like catalyst for methylene blue degradation, *J. Mater. Sci.* 53 (2018) 15081–15095.
- [23] J.F. Perez-Benito, Reaction pathways in the decomposition of hydrogen peroxide catalyzed by copper(II), *J. Inorg. Biochem.* 98 (2004) 430–438.
- [24] C. Walling, A. Goosen, Mechanism of the ferric ion catalyzed decomposition of hydrogen peroxide: effects of organic substrate, *J. Am. Chem. Soc.* 95 (1973) 2987–2991.
- [25] B. Sun, H. Li, X. Li, X. Liu, C. Zhang, H. Xu, X.S. Zhao, Degradation of organic dyes over Fenton-like $\text{Cu}_2\text{O-Cu}/\text{C}$ catalysts, *Ind. Eng. Chem. Res.* 57 (2018) 14011–14021.
- [26] A. Akhundi, A. Habibi-Yangjeh, Graphitic carbon nitride nanosheets decorated with CuCr_2O_4 nanoparticles: novel photocatalysts with high performances in visible light degradation of water pollutants, *J. Colloid Interface Sci.* 504 (2017) 697–710.
- [27] T.T.N. Phan, A.N. Nikoloski, P.A. Bahri, D. Li, Heterogeneous photo-Fenton degradation of organics using highly efficient Cu-doped LaFeO_3 under visible light, *J. Ind. Eng. Chem.* 61 (2018) 53–64.
- [28] L. Guo, F. Chen, X. Fan, W. Cai, J. Zhang, S-doped $\alpha\text{-Fe}_2\text{O}_3$ as a highly active heterogeneous Fenton-like catalyst towards the degradation of acid orange 7 and phenol, *Appl. Catal. B Environ.* 96 (2010) 162–168.
- [29] Y. Gong, X. Zhao, H. Zhang, B. Yang, K. Xiao, T. Guo, J. Zhang, H. Shao, Y. Wang, G. Yu, MOF-derived nitrogen doped carbon modified $g\text{-C}_3\text{N}_4$ heterostructure composite with enhanced photocatalytic activity for bisphenol A degradation with peroxydisulfate under visible light irradiation, *Appl. Catal. B Environ.* 233 (2018) 35–45.
- [30] M.-Q. Wang, W.-H. Yang, H.-H. Wang, C. Chen, Z.-Y. Zhou, S.-G. Sun, Pyrolyzed Fe–N–C composite as an efficient non-precious metal catalyst for oxygen reduction reaction in acidic medium, *ACS Catal.* 4 (2014) 3928–3936.
- [31] L. Lyu, L. Zhang, Q. Wang, Y. Nie, C. Hu, Enhanced Fenton catalytic efficiency of gamma-Cu– Al_2O_3 by sigma- Cu^{2+} -ligand complexes from aromatic pollutant degradation, *Environ. Sci. Technol.* 49 (2015) 8639–8647.
- [32] W. Zhao, C. Liang, B. Wang, S. Xing, Enhanced photocatalytic and Fenton-like performance of CuO_x -decorated ZnFe_2O_4 , *ACS Appl. Mater. Interfaces* 9 (2017) 41927–41936.
- [33] S. Sehati, M.H. Entezari, Sono-incorporation of CuO nanoparticles on the surface and into the mesoporous hexatitanate layers: enhanced Fenton-like activity in degradation of orange-G at its neutral pH, *Appl. Surf. Sci.* 399 (2017) 732–741.
- [34] H. Li, C. Shan, B. Pan, Fe(III)-doped $g\text{-C}_3\text{N}_4$ mediated peroxydisulfate activation for selective degradation of phenolic compounds via high-valent iron-oxo species, *Environ. Sci. Technol.* 52 (2018) 2197–2205.
- [35] J. Ma, Q. Yang, Y. Wen, W. Liu, Fe- $g\text{-C}_3\text{N}_4$ /graphitized mesoporous carbon composite as an effective Fenton-like catalyst in a wide pH range, *Appl. Catal. B Environ.* 201 (2017) 232–240.
- [36] L. Muniandy, F. Adam, A.R. Mohamed, A. Iqbal, N.R.A. Rahman, Cu^{2+} coordinated graphitic carbon nitride ($\text{Cu-g-C}_3\text{N}_4$) nanosheets from melamine for the liquid phase hydroxylation of benzene and VOCs, *Appl. Surf. Sci.* 398 (2017) 43–55.
- [37] Y. Li, H. Xu, S. Ouyang, D. Lu, X. Wang, D. Wang, J. Ye, In situ surface alkalized $g\text{-C}_3\text{N}_4$ toward enhancement of photocatalytic H_2O_2 evolution under visible-light irradiation, *J. Mater. Chem. A* 4 (2016) 2943–2950.
- [38] W. Iqbal, C. Dong, M. Xing, X. Tan, J. Zhang, Eco-friendly one-pot synthesis of well-adorned mesoporous $g\text{-C}_3\text{N}_4$ with efficiently enhanced visible light photocatalytic activity, *Cat. Sci. Technol.* 7 (2017) 1726–1734.
- [39] W. Dong, J. Shi, L. Xu, J. Zhong, J. Duan, Y. Zhang, Synthesis, crystal structure and infrared spectra of Cu(II) and Co(II) complexes with 4,4-dichloro-2,2-(ethylene dioxybis(nitriolmethylidene)diphenol), *Appl. Organomet. Chem.* 22 (2008) 89–96.
- [40] S. Tonda, S. Kumar, S. Kandula, V. Shanker, Fe-doped and -mediated graphitic carbon nitride nanosheets for enhanced photocatalytic performance under natural sunlight, *J. Mater. Chem. A* 2 (2014) 6772.
- [41] T. Xiong, W. Cen, Y. Zhang, F. Dong, Bridging the $g\text{-C}_3\text{N}_4$ interlayers for enhanced photocatalysis, *ACS Catal.* 6 (2016) 2462–2472.
- [42] L. Ge, C. Han, J. Liu, Y. Li, Enhanced visible light photocatalytic activity of novel polymeric $g\text{-C}_3\text{N}_4$ loaded with Ag nanoparticles, *Appl. Catal. A Gen.* 409–410 (2011) 215–222.
- [43] L. Ai, C. Zhang, L. Li, J. Jiang, Iron terephthalate metal-organic framework: revealing the effective activation of hydrogen peroxide for the degradation of organic dye under visible light irradiation, *Appl. Catal. B Environ.* 148–149 (2014) 191–200.
- [44] L. Lyu, D. Yan, G. Yu, W. Cao, C. Hu, Efficient destruction of pollutants in water by a dual-reaction-center Fenton-like process over carbon nitride compounds-complexed Cu(II)-CuAlO_2 , *Environ. Sci. Technol.* 52 (2018) 4294–4304.
- [45] J. Liao, H. Li, X. Zhang, D. Xiao, N. Qiang, Facile fabrication of Ti supported CuO film composed of bamboo-leaf-like nanosheets and their high catalytic performance in the oxidative degradation of methylene blue with hydrogen peroxide, *Appl. Catal. A Gen.* 491 (2015) 94–99.
- [46] W. Luo, L. Zhu, N. Wang, H. Tang, M. Cao, Y. She, Efficient removal of organic pollutants with magnetic nanoscaled BiFeO_3 as a reusable heterogeneous Fenton-like catalyst, *Environ. Sci. Technol.* 44 (2010) 1786–1791.
- [47] J.H. Ramirez, F.J. Maldonado-Ho'dar, A.F. Pe'rez-Cadenas, C. Moreno-Castilla, C.A. Costa, L.M. Madeira, Azo-dye Orange II degradation by heterogeneous Fenton-like reaction using carbon-Fe catalysts, *Appl. Catal. B Environ.* 75 (2007) 312–323.
- [48] Y. Ahmed, Z. Yaakob, P. Akhtar, Degradation and mineralization of methylene blue using a heterogeneous photo-Fenton catalyst under visible and solar light irradiation, *Cat. Sci. Technol.* 6 (2016) 1222–1232.
- [49] C. Chen, Y. Zhou, N. Wang, L. Cheng, H. Ding, $\text{Cu}_2(\text{OH})\text{PO}_4/g\text{-C}_3\text{N}_4$ composite as an efficient visible light-activated photo-Fenton photocatalyst, *RSC Adv.* 5 (2015) 95523–95531.
- [50] C. Lai, M.-M. Wang, G.-M. Zeng, Y.-G. Liu, D.-L. Huang, C. Zhang, R.-Z. Wang, P. Xu, M. Cheng, C. Huang, H.-P. Wu, L. Qin, Synthesis of surface molecular imprinted $\text{TiO}_2/\text{graphene}$ photocatalyst and its highly efficient photocatalytic degradation of target pollutant under visible light irradiation, *Appl. Surf. Sci.* 390 (2016) 368–376.
- [51] X. Zhang, Y. Ding, H. Tang, X. Han, L. Zhu, N. Wang, Degradation of bisphenol A by hydrogen peroxide activated with CuFeO_2 microparticles as a heterogeneous Fenton-like catalyst: efficiency, stability and mechanism, *Chem. Eng. J.* 236 (2014) 251–262.
- [52] S. Li, S. Shi, G. Huang, Y. Xiong, S. Liu, Synergetic tuning charge dynamics and potentials of Ag_3PO_4 photocatalysts with boosting activity and stability by facile in-situ fluorination, *Appl. Surf. Sci.* 455 (2018) 1137–1149.
- [53] S. Liu, D. Li, H. Sun, H.M. Ang, M.O. Tade, S. Wang, Oxygen functional groups in graphitic carbon nitride for enhanced photocatalysis, *J. Colloid Interface Sci.* 468 (2016) 176–182.
- [54] C. Yang, Q. Li, L. Tang, K. Xin, A. Bai, Y. Yu, Synthesis, photocatalytic activity, and photogenerated hydroxyl radicals of monodisperse colloidal ZnO nanospheres, *Appl. Surf. Sci.* 357 (2015) 1928–1938.
- [55] H. Yi, D. Huang, L. Qin, G. Zeng, C. Lai, M. Cheng, S. Ye, B. Song, X. Ren, X. Guo, Selective prepared carbon nanomaterials for advanced photocatalytic application in environmental pollutant treatment and hydrogen production, *Appl. Catal. B Environ.* 239 (2018) 408–424.
- [56] S. Anandan, M. Miyauchi, Ce-doped ZnO ($\text{Ce}_x\text{Zn}_{1-x}\text{O}$) becomes an efficient visible-light-sensitive photocatalyst by co-catalyst (Cu^{2+}) grafting, *Phys. Chem. Chem. Phys.* 13 (2011) 14937–14945.
- [57] Q. Dong, Y. Chen, L. Wang, S. Ai, H. Ding, Cu-modified alkalized $g\text{-C}_3\text{N}_4$ as photocatalytically assisted heterogeneous Fenton-like catalyst, *Appl. Surf. Sci.* 426 (2017) 1133–1140.